HHS Public Access

Author manuscript

Adv Healthc Mater. Author manuscript; available in PMC 2023 April 01.

Published in final edited form as:

Adv Healthc Mater. 2022 April ; 11(8): e2102185. doi:10.1002/adhm.202102185.

De novo design of a membrane-anchored probe for multi-dimensional quantification of endocytic dynamics

Kangqiang Qiu[a],+, **Ryo Seino**[b],+, **Guanqun Han**[c], **Munetaka Ishiyama**[b], **Yuichiro Ueno**[b], **Zhiqi Tian**[a], **Yujie Sun**[c], **Jiajie Diao**[a]

[a]Department of Cancer Biology, College of Medicine, University of Cincinnati, Cincinnati, OH 45267, USA

[b]Dojindo Laboratories, Kumamoto, 861-2202, Japan.

[c]Department of Chemistry, University of Cincinnati, Cincinnati, OH 45221, USA

Abstract

As a process of cellular uptake, endocytosis, with gradient acidity in different endocytic vesicles, is vital for the homeostasis of intracellular nutrients and other functions. To study the dynamics of endocytic pathway, a membrane-anchored pH probe, **ECGreen** was synthesized to visualize endocytic vesicles under structured illumination microscopy (SIM), a super-resolution technology. Being sensitive to acidity with increasing fluorescence at low pH, **ECGreen**, can differentiate early and late endosomes as well as endolysosomes. Meanwhile, membrane-anchoring not only improves the durability of **ECGreen**, but also provides an excellent anti-photobleaching property for long-time imaging with SIM. Moreover, by taking these advantages of **ECGreen**, a multi-dimensional analysis model containing spatial, temporal, and pH information was successfully developed for elucidating the dynamics of endocytic vesicles and their interactions with mitochondria during autophagy, and revealed a fast conversion of endosomes near the plasma membrane.

Graphical Abstract

jiajie.diao@uc.edu; yujie.sun@uc.edu.

+These authors contributed equally to this work.

Author Contributions

J.D. and Y.S. conceived and supervised the whole project. R.S., M.I., and Y.U. designed and synthesized **ECGreen**, and performed the cell experiments with confocal microscope. K.Q. finished the images under SIM. G.H. conducted the theoretical computations. Z.T. helped to analyze the data. All authors were involved in the writing of the manuscript and approved its submission. K.Q, and R.S. contributed equally to this project.

Supporting Information

Supporting Information is available from the Wiley Online Library or from the author.

Conflict of interest

Ryo Seino, Munetaka Ishiyama, and Yuichiro Ueno are employees of Dojindo Laboratories, manufacturer of **ECGreen**.

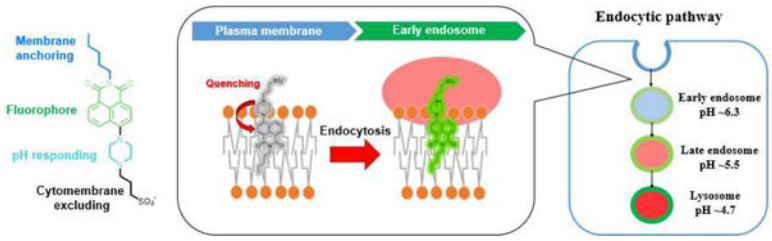

A membrane-anchored pH probe, with excellent durability and photostability in living cells, was developed to study the endocytic dynamics and its interaction with other organelles under nanoscopic visualization.

Keywords

endocytosis; super-resolution imaging; pH probes; multi-dimensional models; membrane anchor

1. Introduction

As one of the most important species, hydronium, also called proton, plays a critical role in many biological functions, including muscle contraction, ion transport, endocytosis, multidrug resistance, proliferation and apoptosis.[1] The change of proton concentration can make the intracellular pH (pH_i) fluctuation, and abnormal pH_i values are closely related to illogical cellular processes which lead to diseases such as Alzheimer's and cancer.[2] The pH_i plays important roles in the organelles' functions, and low pH in lysosomes helps to activate enzyme and protein functions for degradation and the alkalescence makes mitochondria to work regularly.[3] Cellular dysfunction is often associated with abnormal pH values in organelles and hence monitoring pH dynamics of the organelles can help to study the pathological processes.

Fluorescence imaging can help to measure the pH values of organelles using organelles-targeting pH probes.[4] Usually, pH probes are designed based on the special features of the organelles in living cells, such as the acidic environment of lysosomes and the high negative membrane potential of mitochondria.[5] Once the organelles are in an abnormal status, most pH probes will lose their targets and leave the organelles. Therefore, the design of new pH probes that are not affected by the targeting features has attracted great attention.

Endocytosis is a cellular process in which macromolecules are absorbed by plasma membrane-derived vesicles called endosomes.[6] Endocytosis refers to pinocytosis and phagocytosis, and pinocytosis can be divided into macropinocytosis, caveolin- or clathrin-mediated endocytosis, and caveolin- and clathrin-independent endocytosis. Vesicles for the endocytic path, including endosomes (i.e., early endosomes and late endosomes) and endolysosomes, have low pH values from 6.3 to 4.7.[7] The acidic microenvironment can help to maintain the endocytic function of intracellular homeostasis by introducing various nutrients into cells and transporting unwanted components to lysosomes, which collectively act as a waste disposal system.[8] Recent findings also have found that the disruption of endocytosis is related to certain neurodegenerative disorders and immune diseases.[9]

Studying the acidic endocytic vesicles at the high spatial resolution can help not only to investigate the dynamics of endocytic pathway but also to understand the relationship between the acidic endocytic vesicles and diseases.

Here, we designed and synthesized a membrane-anchored pH probe, **ECGreen**, to visualize endocytic vesicles with structured illumination microscopy (SIM) that can overcome the diffraction limit of conventional fluorescence microscopes (~200 nm).[10] **ECGreen** is a small-molecule membrane-anchored fluorescent probe entering cells via endocytosis. Its fluorescence intensity is enhanced as the acidity of endocytic vesicles increases and thus overcomes the limitations posed by commercial probes for acidic vesicles. Because of membrane anchoring, the probe can stay on the vesicle inner surface stably regardless of pH change and thus effectively avoid the destruction by any reactive species inside the endocytic vesicle, which significantly improves both durability and photostability of **ECGreen** for long time tracking endocytic vesicles. Moreover, based on **ECGreen**, we also developed a new multi-dimensional analysis model by incorporating spatial, temporal, and pH information, which can be applied for systematical study of endocytic dynamics. Through this multi-dimensional analysis with **ECGreen**, we studied the conversation, migration and distribution of endocytic vesicles in live cells and their interaction with mitochondria during autophagy, and discovered a fast conversion of endosomes near the plasma membrane. Our new probe and multi-dimensional analysis pave the way for digitalization of sub-cellular dynamics.

2. Results and Discussion

2.1 Design, Synthesis, and Photophysical Properties

The chemical structure of **ECGreen** is shown in Figure 1a, it contains a 1,8-naphthalimide moiety as a highly sensitive fluorescent group with “Head” for membrane anchoring and “Tail” group moieties for pH responding and cytomembrane excluding. The “Head” pentyl group, with the dicarboximide moiety, has been reported to possess the strongest signal in liposomal or autophagosomal membranes by us.[11] The pH responding moiety, a piperazine group, is well known for making a fluorophore pH-dependent through a photo induced electron transfer (PeT) mechanism or twisted intramolecular charge transfer (TICT) mechanism.[12] In addition, as the sulfonate group displays a pKa < 0, compounds containing sulfonate moieties are permanently negatively charged in physiological buffers, thereby unable to cross the lipid bilayer membrane.[13] Anchored on the outer membrane, **ECGreen** can enter live cells via endocytosis and locate on the inner leaflet of endocytic vesicles (Figure 1b). As the acidity of endocytic vesicles increases, the fluorescence intensity of **ECGreen** is enhanced, that makes it a good probe for tracking the dynamics of endocytic vesicles. The synthetic path of this probe is referred to our reported papers.[11] The identity and purity of the probe were successfully confirmed by the results of ESI-MS, ^{1}H NMR, and HPLC spectra (Figures S1–S3).

To study the photophysical properties, the excitation and emission spectra of **ECGreen** were first collected. As shown in Figure 1c, **ECGreen** has an absorption band between 300 and 500 nm, and a band of 450–650 nm for the emission spectrum. Its fluorescence response to different pH is shown in Figure 1d. Lowering the pH value from 8.5 to 4.0, the

fluorescence intensity of **ECGreen** increases and the pKa is calculated to 6.6 (Figure S4). The quantum yields of the probe are 4% at pH 8.0 and 83% at pH 4.0 (refer to fluorescein isothiocyanate, FITC),[14] with a −21-time enhancement (Figure S5). Given the complex intracellular environment, it is important to ensure the probe's high specificity towards pH change. Control experiments using other essential ions and biologically chemicals confirmed that only proton can make **ECGreen** light up (Figure S6). In addition, the pH reversibility study showed the fluorescence of **ECGreen** has no change at the same pH value in different cycle (Figure S7), indicating the probe can be used for illustrating pH changes.

2.2 Calculation of Electronic Structure

Density functional theory (DFT) computation was conducted to aid in the understanding on the electronic structures of **ECGreen** before and after protonation under acidic conditions. As shown in Figure 2a, its highest occupied molecular orbital (HOMO) is primarily located on the electron-donating piperazine and naphthalene side with an energy of −5.74 eV, while its lowest unoccupied molecular orbital (LUMO) centers over the entire naphthalimide structure with an energy of −2.28 eV. Upon protonation at the terminal N of the piperazine unit, no substantial change in the HOMO/LUMO distribution was observed. However, the energies of HOMO and LUMO of the protonated **ECGreen** (**ECGreen-H**) were decreased to −5.83 and −2.35 eV, respectively. More frontier orbitals and energies of **ECGreen** and **ECGreen-H** can be found in Tables S1 and S2. The similar HOMO-LUMO gaps of **ECGreen** before (3.46 eV) and after protonation (3.48 eV) indicate that its UV/visible absorption spectra would not be alternated significantly from neutral to acidic pH, in agreement with reported results of a similar fluorescence probe.[15] Indeed, as shown in Figure 2b, the lowest singlet excited states (S1, primarily from HOMO → LUMO transition) of **ECGreen** and **ECGreen-H** were calculated to be located at 411.2 and 405.6 nm, respectively (Tables S3 and S4), well matching the experimentally observed excitation spectra (Figure 1c). Furthermore, the calculated electron density difference maps (EDDMs) of their S1 states are consistent with the distribution of frontier orbitals and plotted in Figure 2b as well.

2.3 Improved Durability for Super-Resolution Imaging

We first tested some basic properties of ECGreen in live cells. The highly water-soluble tetrazolium salt WST-8 in Cell Counting Kit-8 (CCK-8), can be reduced by dehydrogenase activities for measuring the dehydrogenase activity with NADH in a live cell. The higher dehydrogenase activity indicates higher cell viability. The CCK-8 assay revealed that **ECGreen** was safe for the cells at the different concentrations tested (Figure S8). The longer incubation time was used, the more fluorescent signal inside the cells could be observed (Figure S9). Meanwhile, co-localization analysis with LysoTracker™ Red DND-99 (LTR) (Figure S10) confirmed **ECGreen** localized at the acidic vesicles. The endocytic extracellular vesicles (EVs), labelled with Mem Dye-Deep Red, were used to co-treat with **ECGreen**. The **ECGreen** intensity increased and showed a high overlap with EVs (Figure S11), suggesting the intake of **ECGreen** through endocytosis. To further confirm that **ECGreen** enters cells via endocytosis, we performed experiments by inhibiting the endocytic process. Knowing that low temperature can inhibit endocytosis,[16] we tested

at low temperature and found the decreased fluorescence intensity of **ECGreen** at 4 °C (Figure S12). ECGreen can also work in Jurkat cells (Figure S12a). Meanwhile, we used wortmannin, a potent inhibitor of class I and III PI3-kinases, to block maturation from early to late endosomes (Figure S13a).[17] Co-localization studies (Figure S13) revealed that **ECGreen** co-localized with an early endosomal marker Rab5, a late endosomal marker Rab7, and a lysosomal marker LAMP1, each tagged with RFP (Figure S13c–e). In the presence of wortmannin, RFP–Rab5 showed a ring-shaped structure, indicating a swollen endosome phenotype and location at the endosomal membrane, which are co-localized well with the ring structure observed by **ECGreen** (Figures S13c and S13g). Meanwhiel, RFP–Rab7 and RFP–LAMP1 did not co-localize with the wortmannin-induced ring structure of **ECGreen** (Figures S13d, S13e, S13h and S13i). On the other hand, transferrin-Alexa Flour 546 conjugate, a well-known tracer for the recycling endosome pathway, was co-localized with **ECGreen** signal only in the inhibited condition by wortmannin, indicating that ECGreen is mainly transported to the endo-lysosomal pathway, not the recycling pathway (Figures S13b and S13c). These results suggest that **ECGreen** specifically locates to the early endosomal membrane and then gets transported to the later endo-lysosomal pathway.

SIM offers super-resolution subcellular imaging in living cells with a low background and can overcome the diffraction limit (< 200 nm) of conventional optical microscopes.[18] Figure S14 displays the difference in imaging quality between SIM and widefield microscopy, including that the clearer fluorescent puncta with a lower background were obtained with SIM. The presence or absence of fetal bovine serum (FBS) exerted no obvious effect on the cellular internalization or imaging quality through SIM (Figure S15). By using SIM to acquire images of cells treated with **ECGreen** for longer treatment times, we observed more and brighter puncta (Figures 3a and S16). At the end of the 180-min treatment, the fluorescence puncta exhibited high overlap (86.6%) with the co-stained acidic vesicle dye LTR (Figure S17), which confirmed that **ECGreen** is primarily distributed in acidic vesicles.

The endocytic vesicles including early endosomes, late endosomes, and endolysosomes are all acidic vesicles, for which widely used commercial dyes (e.g., LTR) are membrane-permeable and both lit up and trapped in the acidic microenvironment.[19] However, when the pH changes, the commercial dyes lose their targets and consequently their fluorescence vanishes (Figures 3b,c and S18), which reduces its durability. We then tested the durability of **ECGreen** during the pH fluctuation. An antimalarial drug chloroquine, a cell-permeable base for endolysosomal membrane permeabilization (LMP),[20] and 4% paraformaldehyde, a solution for cell fixation, were used to stimulate live cells for raising the endolysosomal pH value. After treatment, the fluorescence of **ECGreen** remained with a reduced intensity corresponding to pH increase, whereas the signal of LTR had completely vanished (Figures 3d–g and S18). These results demonstrate the improved durability of **ECGreen** for super-resolution imaging.

2.4 Enhanced Photostability for long-time Dynamics Tracking

Anti-photobleaching is an important property of probes that determines whether they can be used for long-time tracking.[21] One of the causes for photobleaching is that reactive

species destroy the structure of the fluorophore. Since it's hard for the reactive species to enter membrane, the membrane insertion should benefit photostability. To confirm this, we did a comparison experiment for the photobleaching time of **ECGreen**, and LTR. Under 100% laser power, the fluorescence of LTR was quickly bleached, while after long irradiation, the fluorescent intensity of **ECGreen** still retained one fifth of its original value (Figures 4a and 4b), thereby showing a much better anti-photobleaching property of **ECGreen**. Next, **ECGreen** was used to track the dynamics of endocytic vesicles with low laser power. The probe maintained 66.20% fluorescence intensity even after 30 images (Figure S19). Thanks to SIM, the dynamics of endocytic vesicles in those images, including the kiss-and-run process, fusion, and fission, were clearly recorded (Figures 4c–4e, Videos S1–S3). Moreover, live HeLa cells labelled with **ECGreen** or LTR were cultured for four days, and the cells were washed with phosphate buffered saline (PBS) three times before and after imaging. The fluorescence of inside acidic probe LTR almost completely disappeared at the second day. In contrast, **ECGreen** can be observed for more than four days (Figures 4d, 4e, and S20). All above results indicate the excellent photostability of **ECGreen.**

2.5 Fast Conversion of Endocytic Vesicles Revealed by a Multi-Dimensional Analysis with ECGreen

For the next stage of quantitative cell biology, the digitization of individual cells and sub-cellular organelles has gained its popularity. However, there is still a lack of systematic methods for digitization. Here, we proposed the concept of a multi-dimensional model, containing various parameters including chemical properties (pH, viscosity, polarity, etc.) as well as spatial-temporal information, etc., for highly efficient analysis. With its pH response and excellent durability and photostability for super-resolution imaging, **ECGreen** was applied to generate a multi-dimensional analysis model for endocytic vesicles. Firstly, without washing, the distance between endocytic vesicles and plasma membrane can be obtained (Figures 5a and S21). Secondly, the fluorescence intensity of **ECGreen** is correlated with the acidity of the vesicles. Finally, by varying treatment time, spatial, temporal, and pH information can be obtained simultaneously and construct a plot (Figure 5b). As shown in Figure 5c, comparing to evenly distributed fluorescent spots at 3 h, the uneven distribution towards plasma membrane at 0.5 h indicates the fast conversion from early to late endosomes near the plasma membrane. After blocking endocytic pathway by wortmannin treatment (Figure 5d), the distribution of fluorescent spots at 0.5 h became even (Figures 5e, S22, and S23). After 3 h, as the result of endosome conversion, the number and intensity of fluorescent spots both increased (Figures S24, S25, and S26), thus confirming that the high intensity spots were associated with late endosomes or endolysosomes with low pH values. These results demonstrate that the multi-dimensional analysis model with **ECGreen** can effectively track endocytic vesicles to uncover unknown biological mechanisms.

2.6 Tracking the Interaction between Endocytic Vesicles and Mitochondria in Autophagy

The interactions of endocytic vesicles with other organelles, such as mitochondria, have been reported to be important for cellular functions.[22] Meanwhile, autophagy is a fundamental process in cellular homeostasis that involves degrading and recycling damaged biomacromolecules or organelles. After autophagosomes engulf damaged

biomacromolecules or organelles, they fuse with endolysosomes to degrade their contents.[23] We then used **ECGreen** and MTDR (MitoTracker™ Deep Red FM) to study the interaction of endocytic vesicles and mitochondria in autophagy. A mitophagy inducer, carbonyl cyanide m-chlorophenylhydrazone (CCCP) was used to damage mitochondria, by which the morphology of mitochondria became fragmented (Figure 6a). Compared to the control group, the number of **ECGreen** fluorescent puncta in the CCCP-treated group increased significantly (Figures S27 and S28). Meanwhile, the Pearson's co-localization coefficient (PCC) value of the interaction increased from 0.96% to 17.12% (Figure 6b), thereby demonstrating the involvement of endocytic vesicles in mitophagy.

In order to track the dynamics of individual endocytic vesicles in autophagy, we then used the above multi-dimension model to analyze the interaction between endolysosomes and mitochondria in mitophagy. Accordingly, we modified the plotting parameters to the distance between endocytic vesicles and mitochondria, and plotted the fluorescent intensity of individual endocytic vesicles with or without CCCP treatment (Figures 6c and S29). As shown in Figure 6d, most endolysosomes were away from mitochondria in the absence of CCCP. In the mitophagy induced by CCCP treatment, almost all endolysosomes moved close to or into mitochondria (Figures 6e), indicating the fusion between endolysosomes and autophagosomes containing damaged mitochondria. Meanwhile, CCCP might induce a pH alteration in the endolysosomes and affect the distribution of **ECGreen** in biomembranes. The above results validate that the multi-dimensional analysis with **ECGreen** is able to catch ongoing cellular process involving endocytic vesicles and other organelles.

3. Conclusion

In sum, we developed **ECGreen**, a pH probe for endocytic vesicles with membrane anchoring and negligible cytotoxicity. Since the fluorescence intensity of **ECGreen** correlates with the acidity, it could distinguish different endocytic vesicles (i.e., early endosomes, late endosomes, and endolysosomes). Because of its excellent durability and photostability induced by membrane anchoring, **ECGreen** is an ideal probe for investigating the dynamics of endocytic vesicles under super-resolution imaging, such as the conversion of endocytic vesicles and the interplay of mitochondria and endocytic vesicles.

In addition, by taking above advantages of **ECGreen**, we also constructed a multi-dimensional analysis for the dynamics of endocytic vesicles and their interactions with other organelles under various conditions. Digitization of biological system is a trend for qualitative cell biology. With the help of a multi-dimensional analysis system, the correlation of various factors could be easily discovered. As a demonstration, through this multi-dimensional analysis with **ECGreen**, we found that early endosomes can quickly convert to late endosomes or even endolysosomes right around the plasma membrane. In the future, combined with big data analysis, this method will significantly improve disease diagnosis and promote drug development.

4. Experimental Section

Materials

All reagents and buffers were purchased from Fujifilm Wako Pure Chemical Corporation, unless otherwise noted. Carbonyl cyanide *m*-chlorophenylhydrazone (CCCP, #C2759) was purchased from Sigma, and MitoTracker™ Deep Red FM (MTDR, #M22426), LysoTracker™ Green DND-26 (LTG, #L7526) and LysoTracker™ Red DND–99 (LTR, #L7528) were purchased from Invitrogen (Thermo Fisher Scientific, USA). Cell Light-Red Fluorescent Protein (RFP) reagents (Thermo Fisher Scientific) were used for staining the early endosome (#C10587), late endosome (#C10589), and lysosome (#C10589). Mem Dye-Deep Red (Dojindo laboratories, #EX03) and PlasMem Bright Red (Dojindo laboratories, #P505) were used for labeling the Extracellular Vesicles (EVs) and for staining the cellular membrane, respectively. All fluorescent dyes were used following the product manuals. Penicillin–streptomycin (#15140163, 10,000 units/mL), fetal bovine serum (FBS, #26140079), and Dulbecco's modified Eagle's medium (DMEM, #11965092) were all purchased from Gibco (Thermo Fisher Scientific, USA). Phosphate-buffered saline (PBS, #SH30256.01) was purchased from Hyclone (GE Healthcare Life Sciences).

Instruments

^{1}H-NMR spectra were recorded on a Bruker AVANCE III HD 400 MHz spectroscopy. Mass spectra were measured with a JMS-T100CS (JEOL), Waters SQD2 (Waters). Fluorescence spectra were measured on an FP-6300 fluorescence spectrophotometer (JASCO). Fluorescence images were obtained by LSM 800 confocal laser scanning microscopy (Zeiss), with excitation at 405 nm (for **ECGreen**), 561 nm (for LTR, RFP and PlasMem Bright Red), and 640 nm (for Mem Dye-Deep Red), using a 500–550-nm filter for **ECGreen**, a 550–650-nm filter for LTR, RFP and PasMem Bright Red, or a 640–760-nm filter for Mem Dye-Deep Red. Theoretical calculations were carried out using ChemOffice Professional 16 (PerkinElmer). HPLC analysis was performed under an isocratic condition (A: H_2O containing 0.1% TFA, B: acetonitrile containing 0.1% TFA; A/B = 60/40) at a flow rate of 1 mL/min using an Inertsil ODS-3 column (250 × 4.6 mm, 5 μm) on a LC-20A (Shimadzu). Absorbance at 254 nm was monitored.

Chemical characteristics of ECGreen

ECGreen (Sodium 3-(4-(1,3-dioxo-2-pentyl-1,3-dihydro-1H-benzo[de]isoquinolin-6-yl)piperazin-1-yl) propansulfonate): ^{1}H-NMR (400 MHz, MeOD) δ: 8.52 (dd, 2H, J = 8.0 Hz), 8.47 (d, 1H, J = 8.0 Hz), 7.80 (t, 1H, J = 8.0 Hz), 7.40 (d, 1H, J = 8.0 Hz), 4.11 (t, 2H, J = 8.0 Hz), 3.47 (s, 4H), 3.38 (s, 4H), 3.21 (s, 2H), 3.02 (t, 2H, J = 8.0 Hz), 3.29–3.22 (m, 2H), 1.74–1.67 (m, 2H), 1.44–1.40 (m, 4H), 0.96–0.93 (m, 3H); ESI-MS: calcd for $[M]^-$, 472.19; found, 472.32.

Spectrophotometric Measurement

The pH-dependent fluorescence intensity of **ECGreen** was measured in 50% DMSO in MES at pH 4.0, 4.5, 5.0, 5.5, 6.0, 6.5, 7.0, 7.5, 8.0 and 8.5, using a fluorescence spectrophotometer (excitation 405 nm, emission 520 nm).

Calculation

All calculations were performed with the Gaussian 16[24] program package employing the DFT method with Becke's three-parameter hybrid functional and Lee-Yang-Parr's gradient corrected correlation functional (B3LYP).[25] 6–31G* basis set was applied for H, C, O, S and N.[26] The geometries of the singlet ground states of compounds were optimized in H_2O using the conductive polarizable continuum model (CPCM). The local minimum on each potential energy surface was confirmed by frequency analysis. Time-dependent DFT calculations produced the singlet excited states of each compound starting from the optimized geometry of the corresponding singlet ground state, using the CPCM method with H_2O as the solvent. The calculated absorption spectra, electronic transition contributions, and electron density difference maps (EDDMs) were generated by GaussSum 3.0.[27] The molecular orbitals were visualized using VMD 1.9.4a51.[28]

Cell culture

The HeLa cell line (cervical cancer cell, a gift from Dr. Carolyn M. Price, University of Cincinnati) and other cell lines were cultured in DMEM containing 10% FBS, 100 units/mL of penicillin, and 100 units/mL of streptomycin in a 5% CO_2 cell incubator (Thermo Fisher Scientific, USA) with 100% humidity at 37 °C.

Isolation of HEK293S-derived EVs and fluorescent labeling

For HEK293S-derived EVs isolation,1.5×10^7 cells were cultured in fresh growth medium for 48h before collecting the supernatant. The resulting conditioned media were centrifuged at 125 × g for 10 min, 10,000 × g for 20 min, and then 100,000 × g for 120 min at 4 °C. Subsequently, the EVs pellets were washed with phosphate-buffered saline (PBS) by ultracentrifugation at 120,000 × g for 120 min at 4 °C. EVs pellets were resuspended in PBS and stored at −80 °C until use. The concentration of the proteins of the EVs were determined using a Micro BCA assay kit. Fluorescent labeling of Evs with Mem Dye-Deep Red was perfomed following the product manuals.

Structured illumination microscopy imaging

All SIM images were performed with a Nikon structured illumination microscopy (N-SIM, version AR5.11.00 64bit, Tokyo, Japan), a 3D-SIM equipped with an Apochromat 100×/1.49 numerical aperture oil-immersion objective lens and solid-state lasers (488 nm, 561 nm, 640 nm, the output powers at the fiber end: 15 mW). Images were captured using Nikon NIS-Elements 512 × 512 using Z-stacks with a step size of 0.2 μm and the raw images were reconstructed and processed with NIS-Elements AR Analysis. Cells were seeded on glass-bottomed culture dishes (MatTek; P35G-1.5–14-C) for 24 h to adhere. **ECGreen** was treated with cells as indication. Commercial dyes staining with 30 min were performed. Before imaging, cells were washed with PBS for 3 times. The green channel images with emission bandwidth at 500–550 nm were excited by a 488 nm laser for **ECGreen**. The red channel images with emission bandwidth at 570–640 nm were excited by a 561 nm laser for LTR. The deep red channel images with emission bandwidth at 660–735 nm were excited by a 640 nm laser for MTDR. All of Pearson's colocalization coefficients (PCC)

were analyzed and quantified in the open-source software CellProfiler. The imaging data analysis was performed with ImageJ.

Cell viability test

Cell Counting Kit-8 (CCK-8, Dojindo Molecular Technologies, Inc., Japan) was used to determine the cytotoxicity of **ECGreen**. HeLa cells were seeded in a 96-well plate with 1×10^4 cells/well. After 24 h to adhere, different concentrations of **ECGreen** were added to the wells and placed in the incubator for 24 h. Then 10 μL of CCK-8 solution was added to each well, the culture plate was incubated for 1 h. Absorbance at 490 nm was determined with the Synergy Mx microplate reader (BioTek Instruments, Inc., USA).

Statistical Analysis

Statistical significance of data was evaluated using Student's *t* test. Data were presented as $M \pm SEM$. $^*p < 0.05$, $^{**}p < 0.01$, and $^{***}p < 0.001$ were considered statistically significant in analyses. Statistics and graphing were performed using Prism 8 (GraphPad) and Excel (Microsoft).

Supplementary Material

Refer to Web version on PubMed Central for supplementary material.

Acknowledgements

We thank Yuki Tatenaka for coordinating this project. J.D. was supported by the National Institutes of Health (NIH R35GM128837). K.Q. was supported by the seed grant (202101) of the Center for Chemical Imaging in Biomedicine at the University of Cincinnati. Y.S. acknowledges the support of the National Science Foundation (CHE1955358).

Data Availability Statement

The data that support the findings of this study are available from the corresponding authors upon reasonable request

References

[1]. a)Gottlieb RA, Dosanjh A, Proc. Natl. Acad. Sci. U. S. A 1996, 93, 3587–3591; [PubMed: 8622979] b)Chin ER, Allen DG, J. Physiol 1998, 512, 831–840; [PubMed: 9769425] c)Varadi A, Rutter GA, Endocrinology 2004, 145, 4540–4549; [PubMed: 15217981] d)Han J, Burgess K, Chem. Rev 2010, 110, 2709–2728; [PubMed: 19831417] e)Steinegger A, Wolfbeis OS, Borisov SM, Chem. Rev 2020, 120, 12357–12489. [PubMed: 33147405]

[2]. a)Izumi H, Torigoe T, Ishiguchi H, Uramoto H, Yoshida Y, Tanabe M, Ise T, Murakami T, Yoshida M. Nomoto, Kohno K, Cancer Treat. Rev 2003, 29, 541–549; [PubMed: 14585264] b)Davies TA, Fine RE, Johnson RJ, Levesque CA, Rathbun WH, Seetoo KF, Smith SJ, Strohmeier G, Volicer L, Delva L, Simons ER, Biochem. Biophys. Res. Commun 1993, 194, 537–543; [PubMed: 8333868] c)Hamilton GRC, Sahoo SK, Kamila S, Singh N, Kaur N, Hyland BW, Callan JF, Chem. Soc. Rev 2015, 44, 4415–4432; [PubMed: 25742963] d)Yin J, Hu Y, Yoon J, Chem. Soc. Rev 2015, 44, 4619–4644 [PubMed: 25317749]

[3]. a)Casey JR, Grinstein S, Orlowski J, Nat. Rev. Mol. Cell Biol 2010, 11, 50–61; [PubMed: 19997129] b)Davidson SM, Heiden MGV, Annu. Rev. Pharmacol. Toxicol 2017, 57, 481–507; [PubMed: 27732799] c)Qiu K, Ke L, Zhang X, Liu Y, Rees TW, Ji L, Diao J, Chao H, Chem. Commun 2018, 54, 2421–2424;d)Fang H, Yao S, Chen Q, Liu C, Cai Y, Geng S, Bai Y, Tian

Z, Zacharias AL, Takebe T, Chen Y, Guo Z, He W, Diao J ACS Nano 2019, 13, 14426–14436; [PubMed: 31799834] e)Qiu K, Du Y, Liu J, Guan J-L, Chao H, Diao J, Theranostics 2020, 10, 6072–6081. [PubMed: 32483439]

[4]. a)Kowada T, Maeda H, Kikuchi K, Chem. Soc. Rev 2015, 44, 4953–4972; [PubMed: 25801415] b)Yue Y, Huo F, Lee S, Yin C, Yoon J, Analyst 2017, 142, 30–41.

[5]. a)Xu W, Zeng Z, Jiang J-H, Chang Y-T, Yuan L, Angew. Chem. Int. Ed 2016, 55, 13658–13699;b)Qiu K, Chen Y, Rees TW, Ji L, Chao H, Coord. Chem. Rev 2019, 378, 66–86;c)Qiu K, Zhu H, Rees TW, Ji L, Zhang Q, Chao H, Coord. Chem. Rev 2019, 378, 66–86.

[6]. Huotari J, Helenius A, EMBO J 2011, 30, 3481–3500. [PubMed: 21878991]

[7]. a)Raiborg C, Wenzel EM, Stenmark H, EMBO J 2015, 34, 1848–1858; [PubMed: 26041457] b)Eisenberg-Bord M, Shai N, Schuldiner M, Bohnert M, Dev. Cell 2016, 39, 395–409. [PubMed: 27875684]

[8]. a)Brunt L, Scholpp S, Cell Mol. Life Sci 2018, 75, 785–795; [PubMed: 28913633] b)Sorkin A, Zastrow MV, Nat. Rev. Mol. Cell Biol 2009, 10, 609–622. [PubMed: 19696798]

[9]. a)Vidyadhara DJ, Lee JE, Chandra SS, J. Neurochem 2019, 150, 487–506; [PubMed: 31287913] b)Heckmann BL, Teubner BJW, Tummers B, Boada-Romero E, Harris L, Yang M, Guy CS, Zakharenko SS, Green DR, Cell 2019, 178, 536–551. [PubMed: 31257024]

[10]. a)Li D, Shao L, Chen BC, Zhang X, Zhang M, Moses B, Milkie DE, Beach JR, Hammer JA 3rd, Pasham M, Kirchhausen T, Baird MA, Davidson MW, Xu P, Betzig E, Science 2015, 349, aab3500;b)Heintzmann R, Huser T, Chem. Rev 2017, 117, 13890–13908; [PubMed: 29125755] c)Huang X, Fan J, Li L, Liu H, Wu R, Wu Y, Wei L, Mao H, Lal A, Xi P, Tang L, Zhang Y, Liu Y, Tan S, Chen L, Nat. Biotechnol 2018, 36, 451–459; [PubMed: 29644998] d)Wang L, Frei MS, Salim A, Johnsson K, J. Am. Chem. Soc 2019, 141, 2770–2781; [PubMed: 30550714] e)Chen Q, Shao X, Hao M, Guan R, Tian Z, Li M, Wang C, Ji L, Chao H, Guan J-L, Diao J Biomaterials 2020, 250, 120059; [PubMed: 32339858] f)Shao X, Chen Q, Hu L, Tian Z, Liu L, Liu F, Wang F, Ling P, Mao Z-W, Diao J Nano Res 2020, 13, 2149–2155;g)Chen Q, Fang H, Shao X, Tian Z, Geng S, Zhang Y, Fan H, Xiang P, Zhang J, Tian X, Zhang K, He W, Guo Z, Diao J Nat. Commun 2020, 11, 6290; [PubMed: 33293545] h)Fang H, Geng S, Hao M, Chen Q, Liu M, Liu C, Tian Z, Wang C, Takebe T, Guan J-L, Chen Y, Guo Z, He W, Diao J Nat. Commun 2021, 12, 109; [PubMed: 33397937] i)Chen Q, Jin C, Shao X, Guan R, Tian Z, Wang C, Liu F, Ling P, Guan J, Ji L, Wang F, Chao H, Diao J, Small 2018, 14, 1802166;k)Chen Q, Hao M, Wang L, Li L, Chen Y, Shao X, Tian Z, Pfuetzner RA, Zhong Q, Brunger AT, Guan J-L, Diao J, Cell Death Dis 2021, 12, 939. [PubMed: 34645799]

[11]. Iwashita H, Sakurai HT, Nagahora N, Ishiyama M, Shioji K, Sasamoto K, Okuma K, Shimizu S, Ueno Y FEBS Lett 2018, 592, 559–567. [PubMed: 29355929]

[12]. a)Poc P, Gutzeit VA, Ast J, Lee J, Jones BJ, D'Este E, Mathes B, Lehmann M, Hodson DJ, Levitz J, Broichhagen J, Chem. Sci 2020, 11, 7871–7883; [PubMed: 34123074] b)Chi W, Chen J, Qiao Q, Gao Y, Xu Z, Liu X, Phys. Chem. Chem. Phys 2019, 21, 16798–16803. [PubMed: 31329206]

[13]. Kucherak OA, Oncul S, Darwich Z, Yushchenko DA, Arntz Y, Didier P, Mély Y, Klymchenko AS, J. Am. Chem. Soc 2010, 132, 4907–4916. [PubMed: 20225874]

[14]. Liu B, Fletcher S, Avadisian M, Gunning PT, Gradinaru CC, J. Fluoresc 2009, 19, 915–920. [PubMed: 19459035]

[15]. Gan J, Chen K, Chang C-P, Tian H, Dyes. Pigm 2003, 57, 21–28.

[16]. Punnonen E, Ryhänen K, Marjomi VS, Eur. J. Cell Biol 1998, 75, 344–352. [PubMed: 9628320]

[17]. a)Shpetner H, Joly M, Hartley D, Corvera S, J. Cell Biol 1996, 132, 595–605; [PubMed: 8647891] b)Spiro DJ, Boll W, Kirchhausen T, Wessling-Resnick M, Mol. Biol. Cell 1996, 7, 355–367; [PubMed: 8868465] c)Liu K, Jian Y, Sun X, Yang C, Gao Z, Zhang Z, Liu X, Li Y, Xu J, Jing Y, Mitani S, He S, Yang C, J. Cell Biol 2016, 212, 181–198. [PubMed: 26783301]

[18]. a)Chen Q, Shao X, Tian Z, Chen Y, Mondal P, Liu F, Wang F, Ling P, He W, Zhang K, Guo Z, Diao J, Nano Res 2019, 12, 1009–1015;b)Liu L-Y, Fang H, Chen Q, Chan MH-Y, Ng M, Wang K-N, Liu W, Tian Z, Diao J, Mao Z-W, Yam VW-W, Angew. Chem. Int. Ed 2020, 59, 19229–19236.

[19]. Pierzynska-Mach A, Janowski PA, Dobrucki JW, Cytometry A 2014, 85, 729–737. [PubMed: 24953340]

[20]. Liu X, Su Y, Tian H, Yang L, Zhang H, Song X, Foley JW, Anal. Chem 2017, 89, 7038–7045. [PubMed: 28553716]

[21]. Yang Z, Li L, Ling J, Liu T, Huang X, Ying Y, Zhao Y, Zhao Y, Lei K, Chen L, Chen Z, Chem. Sci 2020, 11, 8506–8516. [PubMed: 34094186]

[22]. a)Han Y, Li M, Qiu F, Zhang M, Zhang Y, Nat. Commun 2017, 8, 1307; [PubMed: 29101340] b)Wong YC, Ysselstein D, Krainc D, Nature 2018, 554, 382–386; [PubMed: 29364868] c)Nixon RA, Nat. Med 2013, 19, 983–997; [PubMed: 23921753] d)Levine B, Nature 2007, 446, 745–747. [PubMed: 17429391]

[23]. a)Hurley JH, Schulman BA, Cell 2014, 157, 300–311; [PubMed: 24725401] b)Wang Y, Li Y, Wei F, Duan Y, Trends Biotechnol 2017, 35, 1181–1193; [PubMed: 28916049] c)Dikic I, Elazar Z, Nat. Rev. Mol. Cell Biol 2018, 19, 349–364; [PubMed: 29618831] d)Nakatogawa H, Nat. Rev. Mol. Cell Biol 2020, 21, 439–458. [PubMed: 32372019]

[24]. Frisch MJ, Trucks GW, Schlegel HB, Scuseria GE, Robb MA, Cheeseman JR, Scalmani G, Barone V, Petersson GA, Nakatsuji H, Li X, Caricato M, Marenich AV, Bloino J, Janesko BG, Gomperts R, Mennucci B, Hratchian HP, Ortiz JV, Izmaylov AF, Sonnenberg JL, Williams-Young D, Ding F, Lipparini F, Egidi F, Goings J, Peng B, Petrone A, Henderson T, Ranasinghe D, Zakrzewski VG, Gao J, Rega N, Zheng G, Liang W, Hada M, Ehara M, Toyota K, Fukuda R, Hasegawa J, Ishida M, Nakajima T, Honda Y, Kitao O, Nakai H, Vreven T, Throssell K, Montgomery JA Jr., Peralta JE, Ogliaro F, Bearpark MJ, Heyd JJ, Brothers EN, Kudin KN, Staroverov VN, Keith TA, Kobayashi R, Normand J, Raghavachari K, Rendell AP, Burant JC, Iyengar SS, Tomasi J, Cossi M, Millam JM, Klene M, Adamo C, Cammi R, Ochterski JW, Martin RL, Morokuma K, Farkas O, Foresman JB, Fox DJ, Gaussian 16, Revision C.01, Gaussian, Inc., Wallingford CT, 2019.

[25]. a)Becke AD, Phys. ReV. A: Gen. Phys 1988, 38, 3098–3100; [PubMed: 9900728] b)Becke AD, J. Chem. Phys 1993, 98, 5648–5652;c)Lee C, Yang W, Parr RG, Phys. ReV. B: Condens. Matter Phys 1988, 37, 785–789.

[26]. Hehre WJ, Radom L, Schleyer P. v. R., Pople JA, Ab Initio Molecular Orbital Theory, John Wiley & Sons: New York, 1986.

[27]. O'Boyle NM, Tenderholt AL, Langner KM, J. Comp. Chem 2008, 29, 839–845. [PubMed: 17849392]

[28]. Humphrey W, Dalke A, Schulten K, J. Mol. Graph 1996, 14, 33–38. [PubMed: 8744570]

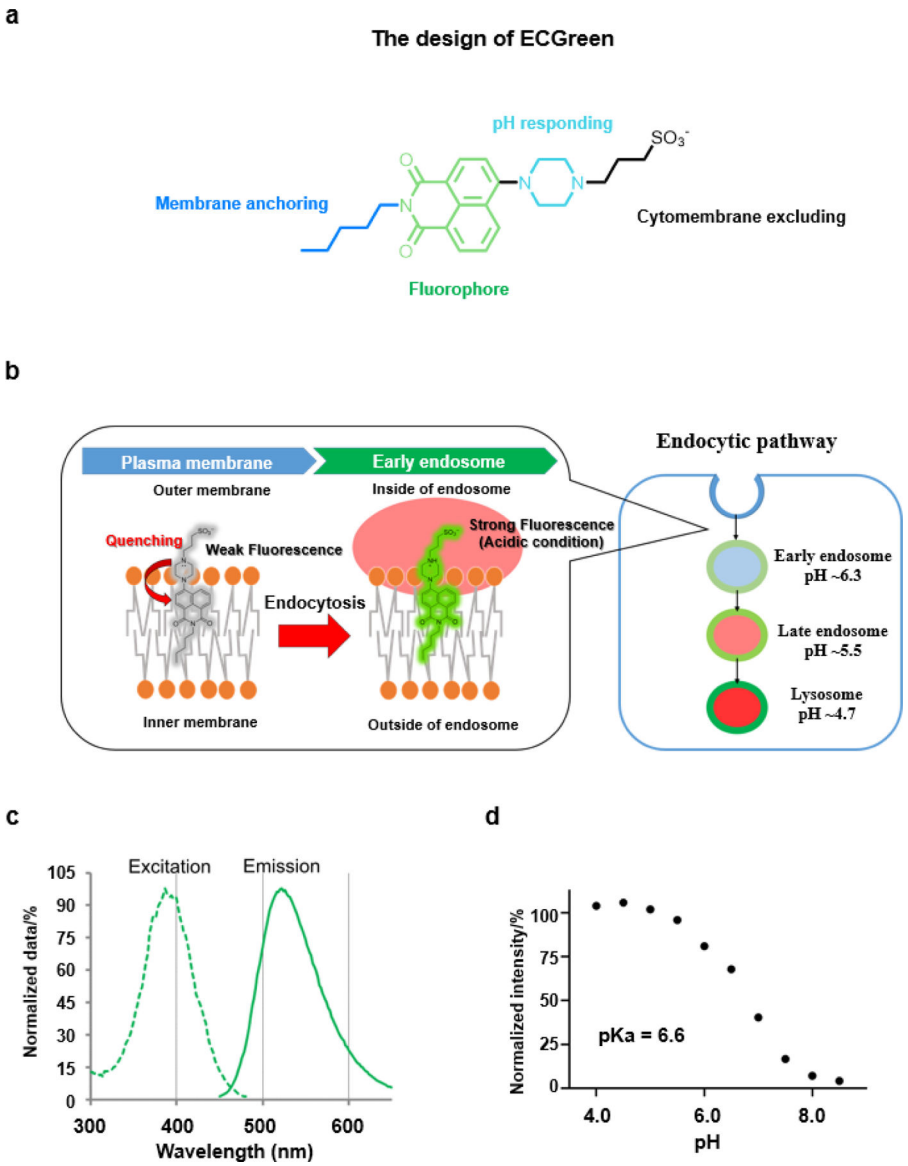

Figure 1.

a) The design of the molecular structure for **ECGreen**. b) The mechanism for visualizing the endocytic pathway. The **ECGreen** probe is a pH- dependent fluorescence dye without membrane permeability. Anchored on the outer membrane, **ECGreen** is internalized via endocytosis and on the inner leaflet of endocytic vesicles. As the acidity of endocytic vesicles increases, the fluorescence intensity of **ECGreen** rises, which makes it a highly specific probe for endocytic vesicles. c) The excitation and emission spectra of **ECGreen**. d) pH-dependent changes of the fluorescence intensity of **ECGreen** (1.0 μM) in buffer solutions (pH 4.0–8.5), excited at 405 nm (emission at 520 nm).

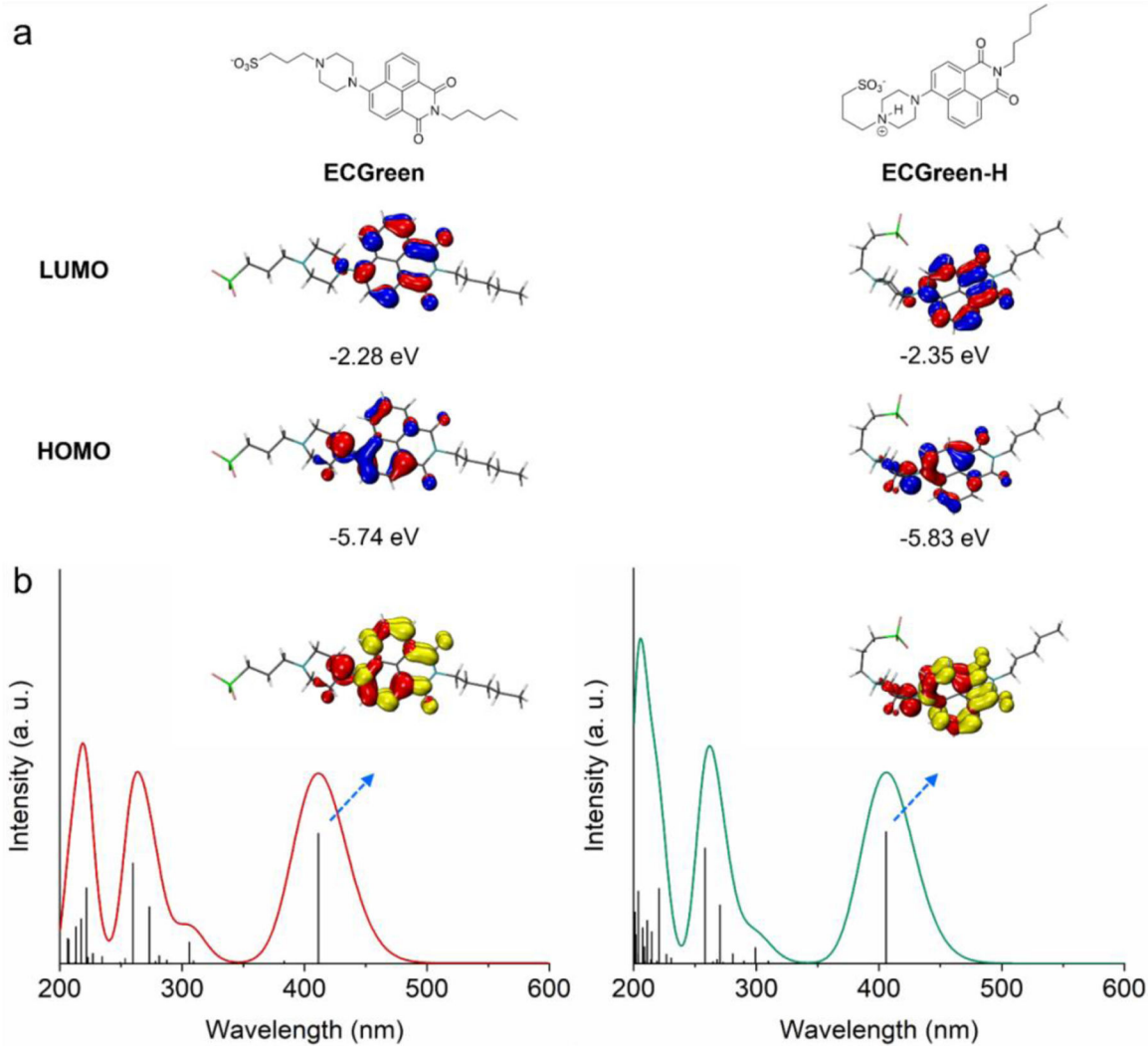

Figure 2.

a) Calculated HOMOs and LUMOs and b) simulated UV-vis absorption spectra and EDDMs of the 1st singlet excited states of **ECGreen** and protonated **ECGreen** (**ECGreen-H**) (red and yellow indicate decrease and increase in electron density, Isovalue = 0.04 for plotting HOMOs, LUMOs, and EDDMs).

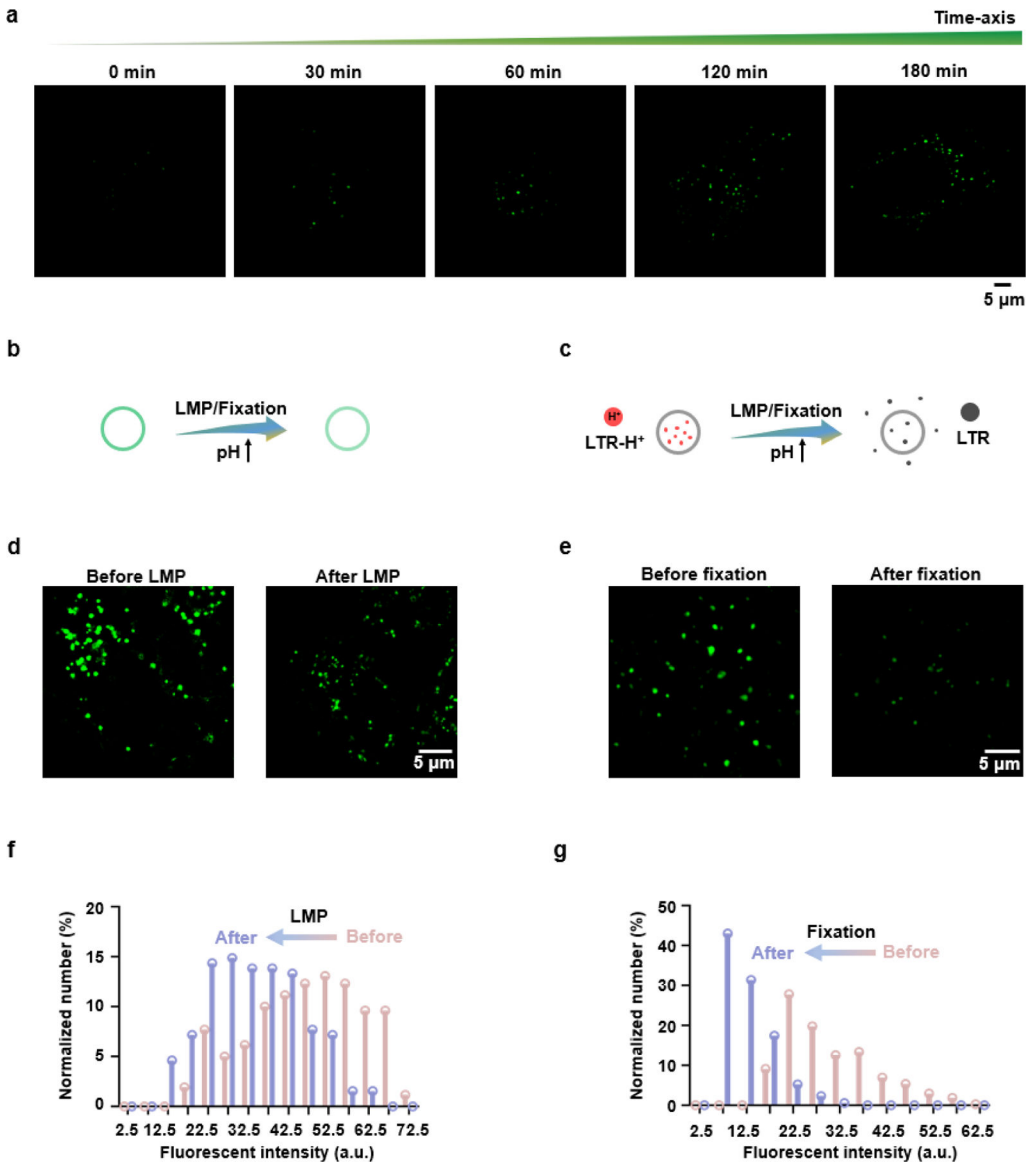

Figure 3.

Super-resolution visualization of acidic endocytic vesicles by **ECGreen**. a) SIM images of HeLa cells labelled with **ECGreen** for different treatment periods. b, c) Schematic illustration of the acidic vesicles labelled with (b) **ECGreen** or (c) LTR during treatments with a higher pH. d) SIM images of HeLa cells labelled with **ECGreen** before and after chloroquine treatment (100 μm, 30 min). e) SIM images of HeLa cells labelled with **ECGreen** before and after 4% paraformaldehyde treatment (20 min). f) The relationship between the number and fluorescence intensity of **ECGreen** before and after LMP. g) The relationship between the number and fluorescence intensity of **ECGreen** before and after fixation.

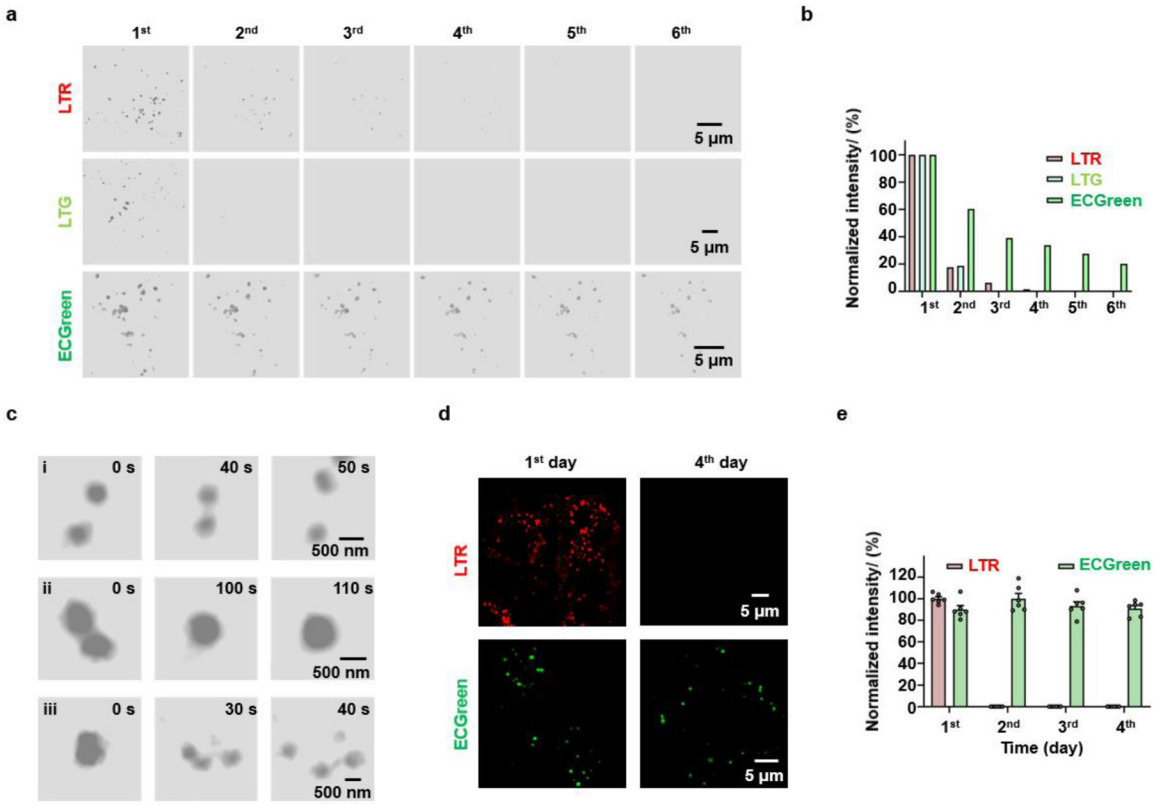

Figure 4.

Continuous imaging of endocytic vesicles. a, b) Continuous imaging of HeLa cells labelled with **ECGreen**, LTR or LTG at the largest laser intensity for photobleaching. The (a) SIM images and (b) normalized fluorescence intensity of **ECGreen**, LTR and LTG. c) Dynamic SIM images of (i) the kiss-and-run process, (ii) fusion, and (iii) fission process of the endocytic vesicles. d) The images of HeLa cells labelled with LTR or **ECGreen** for the first day and the fourth day. e) The normalized fluorescence intensity of LTR or **ECGreen** in HeLa cells at different days.

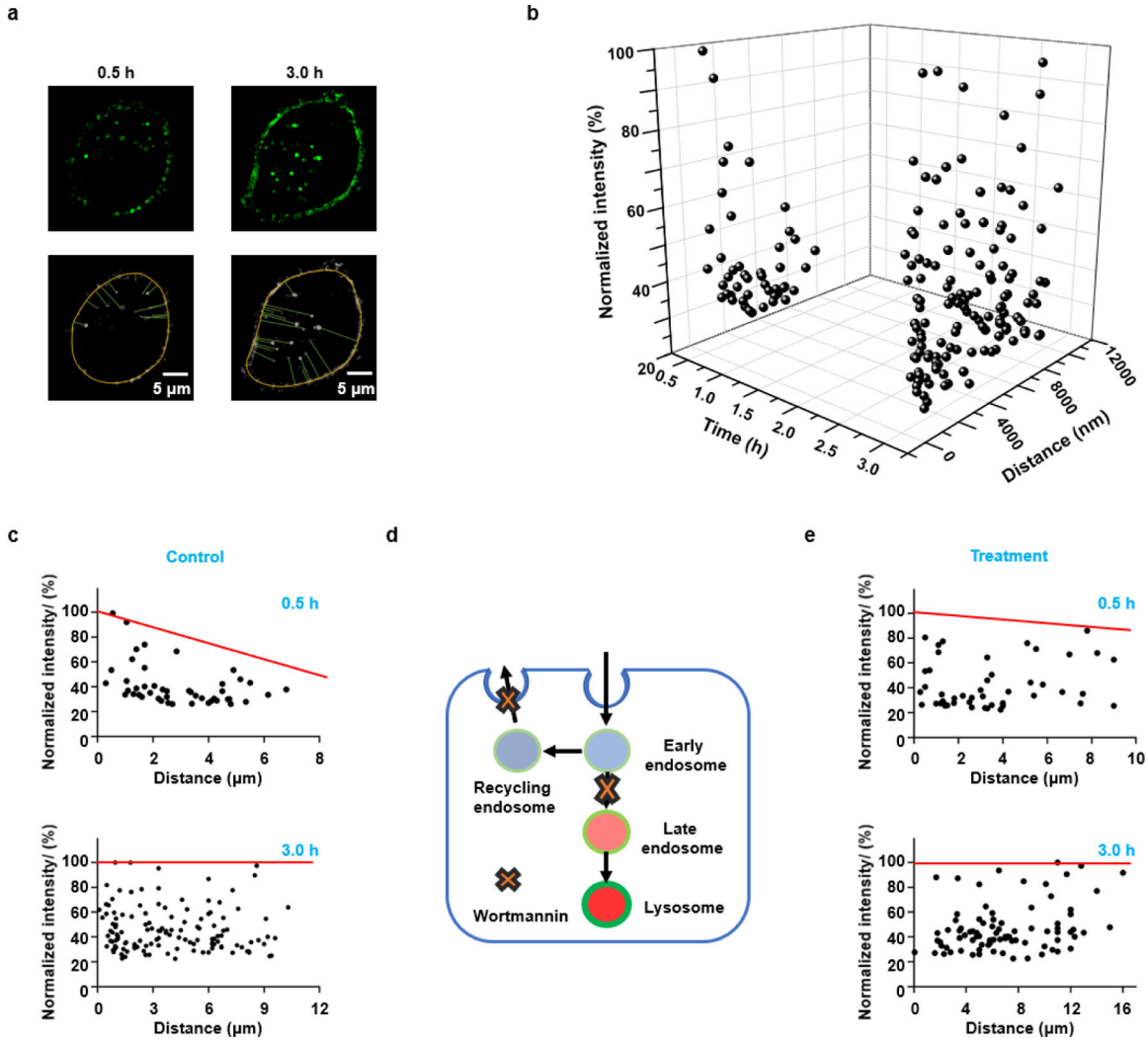

Figure 5.

Constructing a multi-dimensional model for endocytic vesicles with **ECGreen** (5 μM). a) The SIM images of HeLa cells treated with **ECGreen** for 0.5 h and 3 h, and the quantification of distance between endocytic vesicles and cytomembrane. b) A 3-dimensional space for endocytic vesicles. The parameters were time, distance (between endocytic vesicles and plasma membrane), and fluorescence intensity (pH). c) The relationship between distance and fluorescence intensity for the Control group incubated with **ECGreen** for 0.5 h and 3 h. d) Schematic illustration of the effect of wortmannin that inhibits the recycling of endosomes and their conversion to endolysosomes. e) The relationship between distance and fluorescence intensity for the group with the treatment of wortmannin (100 nM, with **ECGreen**) for 0.5 h and 3 h. Red line stands for the tendency of maximum fluorescence intensity for the endocytic vesicles.

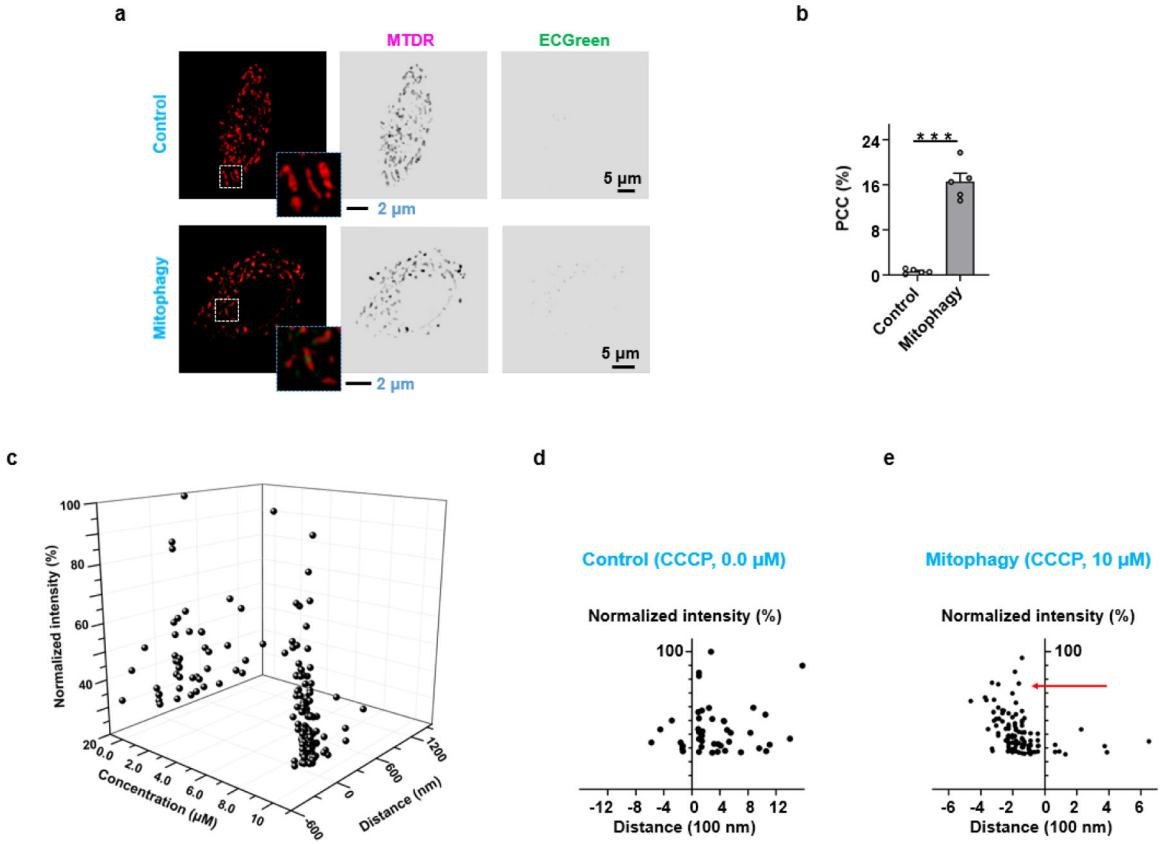

Figure 6.

Endocytic vesicles interacted with mitochondria in live HeLa cells labelled with **ECGreen** and MTDR. The colour of MTDR was false. a) Endocytic vesicles interacting with mitochondria before and after mitophagy. b) PCC values of **ECGreen** and MTDR before and after mitophagy. c) A 3-dimensional space for endocytic vesicles. The parameters were concentration of CCCP, distance (between endocytic vesicles and mitochondria), and fluorescence intensity (pH). d) The relationship between distance and fluorescence intensity for the Control group without CCCP treatment. e) The relationship between distance and fluorescence intensity for the Mitophagy group with CCCP treatment. Data are given as $M \pm SEM$ ($n = 6$); ***$p < 0.001$ compared to control cells.